Physics of the Earth and Planetary Interiors 240 (2015) 105–113

Contents lists available at ScienceDirect

Physics of the Earth and Planetary Interiors

journal homepage: www.elsevier.com/locate/pepi

Magnetic mineralogy of a weathered tropical basalt, Hainan Island, South China

Tingping Ouyang [a,b,*], Zhihua Tang [a,c], Xiang Zhao [b], Chengjing Tian [a,c], Jinlong Ma [a], Gangjian Wei [a], Ningsheng Huang [a], Mingkun Li [a,c], Yong Bian [a,c]

[a] Key Laboratory of Marginal Sea Geology, Guangzhou Institute of Geochemistry, Chinese Academy of Sciences, Guangzhou, Guangdong 510640, People's Republic of China
[b] Research School of Earth Sciences, The Australian National University, Canberra, ACT 0200, Australia
[c] University of Chinese Academy of Sciences, Beijing 100049, People's Republic of China

ARTICLE INFO

Article history:
Received 25 December 2013
Received in revised form 18 December 2014
Accepted 5 January 2015
Available online 12 January 2015

Keywords:
Magnetic minerals
Rock magnetism
Pedogenesis
Basalt weathering
Tropical climate
South China

ABSTRACT

Numerous studies have shown that mineral magnetic properties are sensitive indicators of weathering and soil formation (pedogenesis). However, the formation pathways and subsequent alteration mechanisms of specific weathering products are poorly constrained. We report a detailed magnetic investigation through a basalt profile that has been weathered under tropical conditions in South China. The rock magnetic analyses show that hot and humid conditions led to the neoformation of fine-grained magnetite and promoted mineral transformations in the form of maghemitization and hematization. Thus, although the basaltic parent material is rich in titanomagnetite, the final products of the weathering process are maghemite and hematite. Magnetic grain-size varies through the profile, with a combination of pseudo-single domain and single-domain particles at the base, with fining to single-domain in the middle and a mixture of superparamagnetic and single-domain particles in the uppermost profile. Importantly, the magnetic mineral assemblage through the profile is influenced by the mobilization and migration of iron through the sequence. This process is illustrated by concentration-dependent magnetic parameters, which reach maxima at the assembly depth of major and trace elements and minima at the oxic front where Fe content is its lowest.

1. Introduction

Pedogenesis, the process of soil formation, is a complex mechanism that remains poorly understood. Because of its redox potential, iron is particularly sensitive to processes that occur during pedogenesis, making it an exceptional indicator of soil development and weathering state. The control of weathering on iron oxides (and oxyhydroxides) remains unconstrained (Dearing et al., 1996; Banerjee, 2006; Van Dam et al., 2008; Blundell et al., 2009). Thus, the pathways via which iron minerals are formed and modified in a soil are poorly understood. Weathering perturbations to iron mineralogy result in measurable modifications to a basalt's magnetic properties and on this basis rock magnetic parameters have been used as paleoclimatic proxies (Marshall and cox 1972; Schwertmann 1985; Fine et al., 1989; Morup et al., 1990; Zhou et al., 1990; Maher and Thompson, 1992, 1994, 1995; Koch et al., 1995; Han et al., 1996; Maher et al., 2003; Liu et al., 2005a; Maher 2007; Navarre-Sitchler and Brantley 2007; Borges et al., 2011; Dietze et al., 2011; Long et al., 2011). Moreover, the rock magnetic investigation of basalts has provided key constraints for understanding the Martian environment (Barrón and Torrent, 2002; Gunnlaugsson et al., 2002, 2006; Chevrier et al., 2006).

Previous studies suggested that magnetic susceptibility (κ) is correlated positively with mean annual temperature and precipitation over large geographical regions due to the pedogenic formation of ferrimagnets in temperate, semi-arid environments (Kukla et al., 1988; Heller et al., 1993; Liu et al., 1995, 2012a; Maher, 1998; Porter et al., 2001; Warrier and Shankar, 2009). In some high rainfall regions, however, κ exhibits a negative correlation with precipitation as pedogenic ferrimagnets are transformed to weakly magnetic minerals (Begét et al., 1990; Singer et al., 1996; Chlachula et al., 1998; Liu et al., 2003; Balsam et al., 2004; Yin and Guo, 2006; Hu et al., 2009). Thus, magnetic mineral formation and transformation becomes a key process to understand basalt weathering and pedogenesis.

Mineral magnetism serves as an effective means for deciphering pedogenic processes. The red soil (laterite) in subtropical to tropical southern and southeastern China provides important terrestrial

* Corresponding author at: Key Laboratory of Marginal Sea Geology, Guangzhou Institute of Geochemistry, Chinese Academy of Sciences, Guangzhou, Guangdong 510640, People's Republic of China.

http://dx.doi.org/10.1016/j.pepi.2015.01.001
0031-9201/

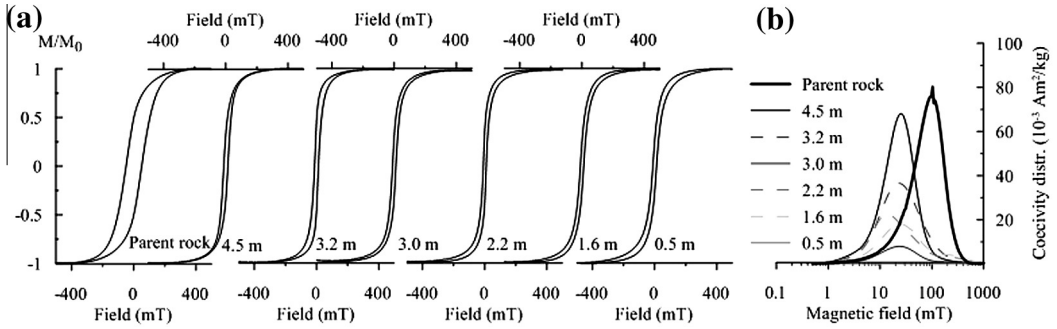

Fig. 1. (a) Hysteresis loops; and (b) coercivity distribution for parent rock and representative weathering samples.

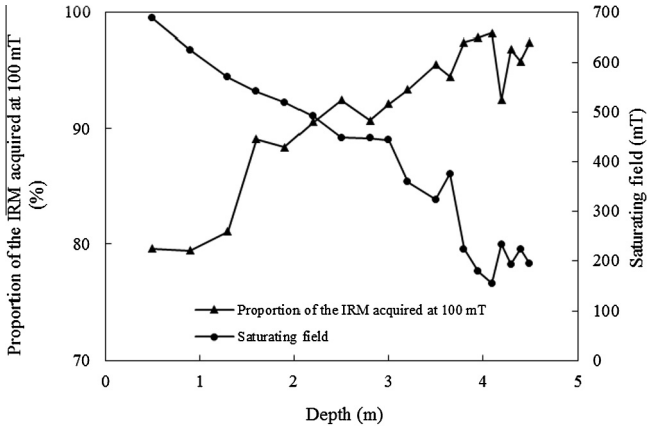

Fig. 2. Proportion of the IRM acquired at 100 mT and loop closing field (mT) variations vs. depth.

archives of palaeoclimate and palaeoenvironment, e.g., Liu et al. (2012b, 2010). We present a detailed environmental magnetic investigation of a basalt weathering profile formed in a tropical climate. The profile is characterized by different zones exhibiting progressive soil formation with respect to depth. The profile is therefore a suitable archive to reconstruct the progression of pedogenic magnetic mineral formation/transformation in basalt weathered in a tropical climate. The main aim of this work is to investigate the magnetic mineral transformation during basalt weathering process. We tend to provide deep understanding of soil environmental magnetism for tropical soil and mineral magnetic basis for magnetic application in weathering soil and laterite in southern China.

2. Materials and methods

2.1. Study area and sampling sites

The studied profile is located on Hainan Island in a tropical climate controlled by the East Asian monsoon. The modern mean annual temperature is ~25 °C, while annual precipitation over the past century has varied from 800 to 2500 mm/y with a mean of ~1500 mm/y. As a result of the monsoon system, precipitation is highly seasonal, with over 80% of the annual rainfall occurring between May and October. The studied profile is located on the north of Hainan Island, where numerous lateritic weathering profiles have developed from basalts (Huang et al., 1993). K-Ar ages date the basalts in this region to ~4.0 Ma (Zhu and Wang, 1989). The location, petrography and sampling of the ~6 m profile examined in this study have been described in detail by Ma et al. (2007) who proposed that it has developed continuously since its formation and that the oxic front and enrichment layer (so-called assembly depth) are located at depths of 2.8–3.0 m and 3.2–3.5 m, respectively. The top ~0.3 m of the profile is composed of loose soil and covered by plants, indicating it may have been disturbed by agricultural activity. Beneath this top layer is an ~0.2 m laterite, which was not sampled because it contains gravels. Seven samples (numbered 1 through 7) were collected from a fine laterite layer with a homogeneous red colour between heights of 0.5 m and 2.5 m (sampling interval of ~30 cm). Between 2.5 and 3.2 m, the profile becomes a little yellowish, but basically remains red. Three samples (numbered 8–10) were collected from this portion of the profile. The sequence becomes pistachio below 3.2 m, with unweathered core stones, and black shell-shaped matter filling the areas between the core stones. Both materials were sampled together at intervals of 10–15 cm to a depth of 4.5 m (numbered 12–20, sample number 11 is missing). A picture of the profile and sampling numbers were shown in Figs. 6 and 7. A sample of fresh tholeiitic basalt, consisting of pyroxene (10%), plagioclase (60%), clinopyroxene (25%) and opaque minerals (mainly ilmenite), was collected from a quarry profile next to the sampling profile (Ma et al., 2007).

All samples were air dried at room temperature and ground into a powder. The sample material was then packed into non-magnetic plastic cubes (8 cm^3) and small gelatin capsules.

2.2. Magnetic analysis

A suite of mineral magnetic analyses was performed on all of the collected samples. Low (976 Hz) and high (15,616 Hz) frequency magnetic susceptibilities (κ_{lf} and κ_{hf}, mass-specific as χ_{lf} and χ_{hf}, respectively) were measured using an AGICO Kappabridge MFK1-FA. Frequency dependence of magnetic susceptibility was calculated as χ_{fd} (%) = $[(\chi_{lf} - \chi_{hf})/\chi_{lf}] \times 100$ (Thompson and Oldfield, 1986). Volume magnetic susceptibility as a function of temperature (κ vs T) were measured from room temperature to 700 °C using CS4/CSL high and low temperature units attached to the MFK1-FA instrument. Anhysteretic remanent magnetizations (ARM) was imparted with a D-2000 alternating demagnetizer creating a 100 mT peak AF and a DC biasing field of 0.05 mT. Saturation isothermal remanent magnetization (SIRM) was acquired in a 2.5 T field with an IM-10–30 pulse magnetizer. The S-ratio was calculated using the equation of Stober and Thompson (1977), based on comparing the SIRM and the remanence created in a 300 mT backfield. Imparted laboratory remanences were measured with an AGICO JR6-A spinner magnetometer. The measurements described above were performed at the Guangzhou Institute of Geochemistry, Chinese Academy of Sciences.

Hysteresis loops with a maximum applied field of 0.5 T, IRM acquisition curves with a maximum applied field of 1.0 T and first-order reversal curves (FORC) were measured using a Princeton Measurements Corp. Micromag 3900 Vibrating Sample Magnetom-

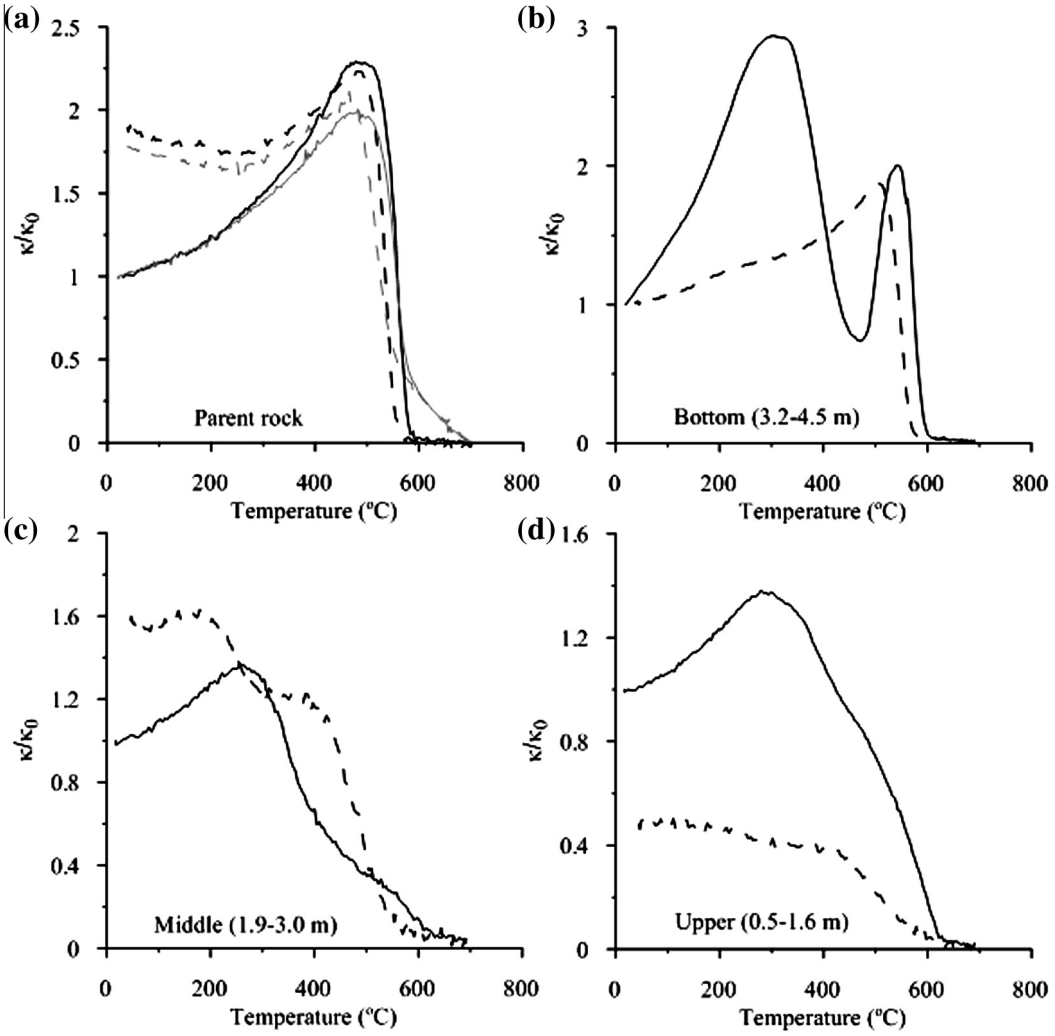

Fig. 3. Magnetic susceptibility variations during heating and cooling process (κ–T curves). Black and grey lines represent argon and air atmosphere, respectively. Solid and dashed lines stand for heating and cooling process, respectively.

eter (VSM) at the Research School of Earth Sciences, Australian National University.

3. Results

3.1. Hysteresis properties

Hysteresis loops exhibit changing shapes through the sampled profile, indicating gradual evolution of the magnetic mineral assemblage (Fig. 1a). The hysteresis loop of parent material sample closes at a field of ~ 300 mT, indicating lower coercivity minerals, such as magnetite, dominate its properties (Fig. 1a). The field at which the hysteresis loops close increases continuously from ~ 120 mT in the lowermost profile with a depth of 4.5 m to ~ 400 mT in the uppermost profile with a depth of 0.5 m. This pattern demonstrates that the relative contribution of high coercivity components to the magnetic mineral assemblage increases from the bottom to the top of the profile.

3.2. IRM acquisition curve

In a similar manner to the hysteresis loops (Fig. 1a), the IRM acquisition curves (coercivity distribution illustrated in Fig. 1b) reveal varying magnetic hardness through the profile. Specifically, the proportion of the IRM acquired at 100 mT decreases and the magnitude of the loop closing field (mT) increases from the base to the top layer of the profile (Fig. 2). These variations again indicate that concentration of high coercivity components increases from the bottom to the top of the profile.

3.3. κ–T curves

The air and argon atmosphere thermomagnetic curves for the parent material have similar characteristics up to 500 °C with κ increasing continuously, which mainly corresponds to the combination of low-Ti substituted spinel and the unblocking of some SD particles, with a significant decrease at the Curie temperature of magnetite (Zhou et al., 1997; Liu et al., 2005b; Chevrier et al., 2006; Petrovsky and Kapicka, 2006) (Fig. 3a). Heating in air produces a high temperature signal (above 600 °C) corresponding to hematite. Such a signal is absent from the argon atmosphere curve, indicating that the hematite must be produced during heating in air (Deng et al., 2004; Zhang et al., 2012). Ho et al. (2000) suggested that basalts in this area contain both titanomagnetite and ilmenite. Therefore, it can be deduced that the magnetic mineral composition of the parent rock should be a minor magnetite component and a dominant titanium-poor titanomagnetite component.

The heating curves of all the profile samples contain peaks at ~300 °C (Fig. 3) with subsequent decreases at higher temperatures. Decreasing κ is interpreted as a signature of metastable maghe-

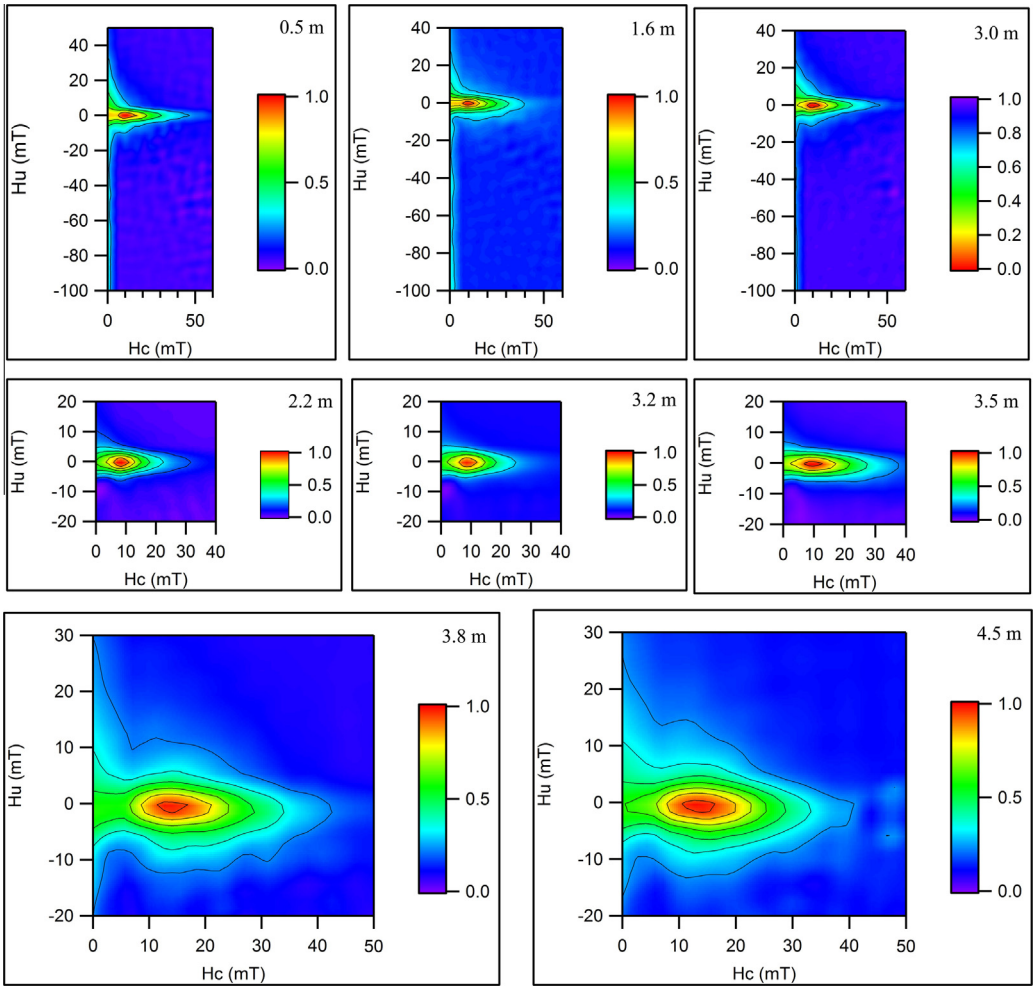

Fig. 4. FORC diagrams for representative samples from the studied weathering profile. 182 FORCs were measured for each FORC diagram and smoothing factor 4 was used in the calculation of each distribution. Numbers within the diagrams are the depths of measured samples.

mite (γ-Fe_2O_3) inverting to weakly magnetic hematite (α-Fe_2O_3). In addition, all of the samples from the profile contain a magnetite Curie point (Fig. 3) (Deng et al., 2005; Liu et al., 2005b; Lattard et al., 2006; Petrovsky and Kapicka, 2006).

Samples from the lower parts of the profile exhibit a decrease in κ between 330 and 470 °C, followed by an increase between 470 and 540 °C (Fig. 3b), which is typical of titanomaghemite inversion (O'Donovan and O'Reilly, 1977; Özdemir, 1987; Bina and Prevot 1989). Given the composition of the parent material, this titanomaghemite is expected to be low temperature oxidation product originating from the original titanomagnetite (Bleil and Petersen 1983; De Oliveira et al., 2002; Oliva-Urcia et al., 2011). In contrast, titanomaghemite inversion is not observed in the samples from the middle and upper parts of the profile (Fig. 3c and d). Instead a clear hematite component can be identified in these heating curves above 600 °C (Chevrier et al., 2006; Soubrand-Colin et al., 2009; Liu et al., 2012b). Moreover, a new phase with a curie temperature of ~550 °C was identified from the cooling curve of Fig. 3c. According to the research of Jiang et al. (2014), this new magnetic phase may be Al-substituted magnetite. This new Al–magnetite should be the production of the reaction of original hematite and clay minerals during high temperature thermal treatment (Zhang et al., 2012).

Variations in magnetic susceptibility variation during heating and cooling exhibit a variety of forms and the samples (excluding the parent material) can be divided into three groups based on their κ–T behaviour. The κ–T curves of samples from the bottom of the weathering profile (depths of 4.5–3.2 m) are all similar with a clear double-peak during heating. Interpretation of these features suggests their magnetic mineral assemblages are dominated by phases characteristic of immature weathering. Samples from the middle (3.0–1.9 m) and the upper parts (1.6–0.5 m) of the section contain products of high and extreme weathering, respectively.

3.4. FORC diagram

First-order reversal curves (FORC) are a class of partial hysteresis loops that can provide information on the coercivity and interaction field distributions in fine particle magnetic systems (Pike et al., 1999, 2001; Roberts et al., 2000). FORC diagrams were produced from the measured FORC curves using the software FORCinel_v1.21 (Hairrison and Feinberg, 2008) for eight samples through the profile. Each sample contains a signature of an SD contribution (Fig. 4). On the basis of the FORC distributions the profile can be separated into two parts. The steep contours close to the origin (B_c values <10 mT) within the FORC distributions of samples from 0.5 m to 3.0 m indicate that the upper parts of the profile contain a substantial SP component. In the middle parts of the profile (3.2–3.5 m), the FORC diagrams indicate a peak that represents noninteracting SD grains (Fig. 4). The combination of a central ridge and asymmetrical vertical spread within the FORC distributions of samples at depths of 3.8 m and 4.5 m suggests a mixture of SD and pseudo-single domain (PSD) particles towards the base of the profile (Roberts et al., 2000; Muxworthy and Dunlop, 2002; Carvallo et al., 2006; Egli et al., 2010) (Fig. 4).

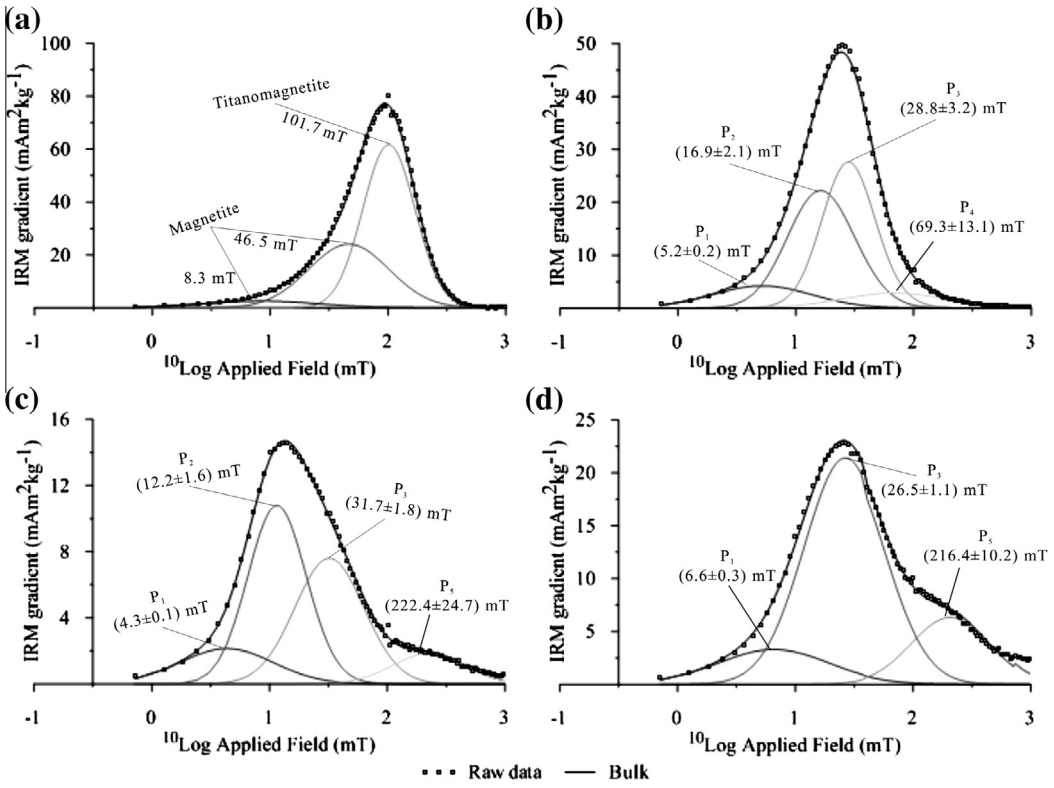

Fig. 5. Possible magnetic mineral compositions of two and four or three main experimentally derived coercivity components coexisting in the parent rock and weathering products, respectively. (a) Parent rock; (b) bottom part (samples 10–20, 3.2–4.5 m); (c) middle part (samples 5–9, 1.9–3.0 m); (d) upper part (samples 1–4, 0.5–1.6 m) of the weathering profile. Component P_1 and P_2 should be pedogenic magnetite with different coercivity and grain size distribution. Component P_3, P_4 and P_5 stand for pedogenic maghemite, pedogenic titanomaghemite and pedogenic hematite, respectively.

4. Discussion

4.1. Magnetic mineralogy transformation

The decomposition of IRM acquisition curves using combinations of cumulative log-Gaussian (CLG) distributions has been shown to be an effective approach to identify the different magnetic mineral phases within a mixed assemblage (Kruiver et al., 2001; Heslop et al., 2002; Spassov et al., 2003). For the parent rock sample, CLG analysis of the measured IRM acquisition curve reveals three coercivity phases (Fig. 5a). The contributions of the individual components to the total IRM are 5%, 36% and 59% with median acquisition fields ($B_{1/2}$) of 8, 47 and 100 mT and dispersion parameters (DP) of 0.49, 0.34 and 0.22. The first two different coercivity components should be the same magnetic mineral with different grain size because the measuring time is shorter than the relaxation time of all SP grains (Heslop et al., 2004). Combing with the results of κ–T curves, it can be speculated that magnetite and titanomagnetite are main magnetic components within the parent material.

The initial magnetite within the parent rock changes to finer grained lower coercivity magnetite (P_1 and P_2 in Fig. 5) and maghemite (P_3 in Fig. 5) due to pedogenesis during the weathering process. With the strength of weathering, this pedogenic magnetite can be oxidized to maghemite or hematite (P_3 and P_5 in Fig. 5). At the early stage of weathering, some titanomagnetite converted to titanomaghemite (P_4 in Fig. 5) due to low temperature oxidation. Variations in the modelled CLG parameters through the section show the IRM characteristics of the weathering products are significantly different from the parent material (Fig. 6).

Compared to the parent rock, the two magnetite components can also be identified as weathering products. The low coercivity component, here defined as superfine magnetite (maybe SSD particles), is present through the whole profile (Fig. 6). The sharp increase in DP exhibited by this superfine component in the upper section of the profile indicates that the grain size tends to be on average finer but with a wider distribution during extreme weathering process (Fig. 6). However, another magnetite with higher $B_{1/2}$, relatively stable DP and the same SIRM pattern to superfine magnetite is absent from the upper section of the profile. The SIRM variation patterns of magnetite and maghemite suggest a maghemitization process during extreme weathering (Fig. 6).

During the early stages of weathering, some titanomagnetite appears to have been converted to titanomaghemite as a result of low temperature oxidation. We noted that pedogenic titanomaghemite only exists within the bottom part (3.2–4.5 m) of the weathering profile. Moreover, the DP value of titanomaghemite exhibits a relatively wide range of DP values (between 0.36 and 0.54) (Fig. 6). This pedogenic titanomaghemite can be changed to ilmenite and maghemite and hematite due to extreme weathering and maghemitization and hematization processes (addition of oxygen or iron departure). Therefore, no titanomaghemite can be identified from the middle and upper parts of the weathering profile (Fig. 6).

The SIRM pattern of maghemite follows the pattern of titanomaghemite and magnetite in the bottom parts (3.2–4.5 m) and middle and upper parts (0.5–3.0 m) of the section, respectively (Fig. 6). It may be concluded that this maghemite is probably from both parental magnetite and titanomaghemite produced during the early stages of weathering. It is noteworthy that SIRM of all components is lowest at the oxic front and increases in the rare earth element (REE) enrichment section (Fig. 6).

The *S*-ratio quantifies the relative abundance of soft (ferri-) and hard (antiferromagnetic) components within a mixed magnetic mineral assemblage (Evans and Heller, 2003; Liu et al., 2012c).

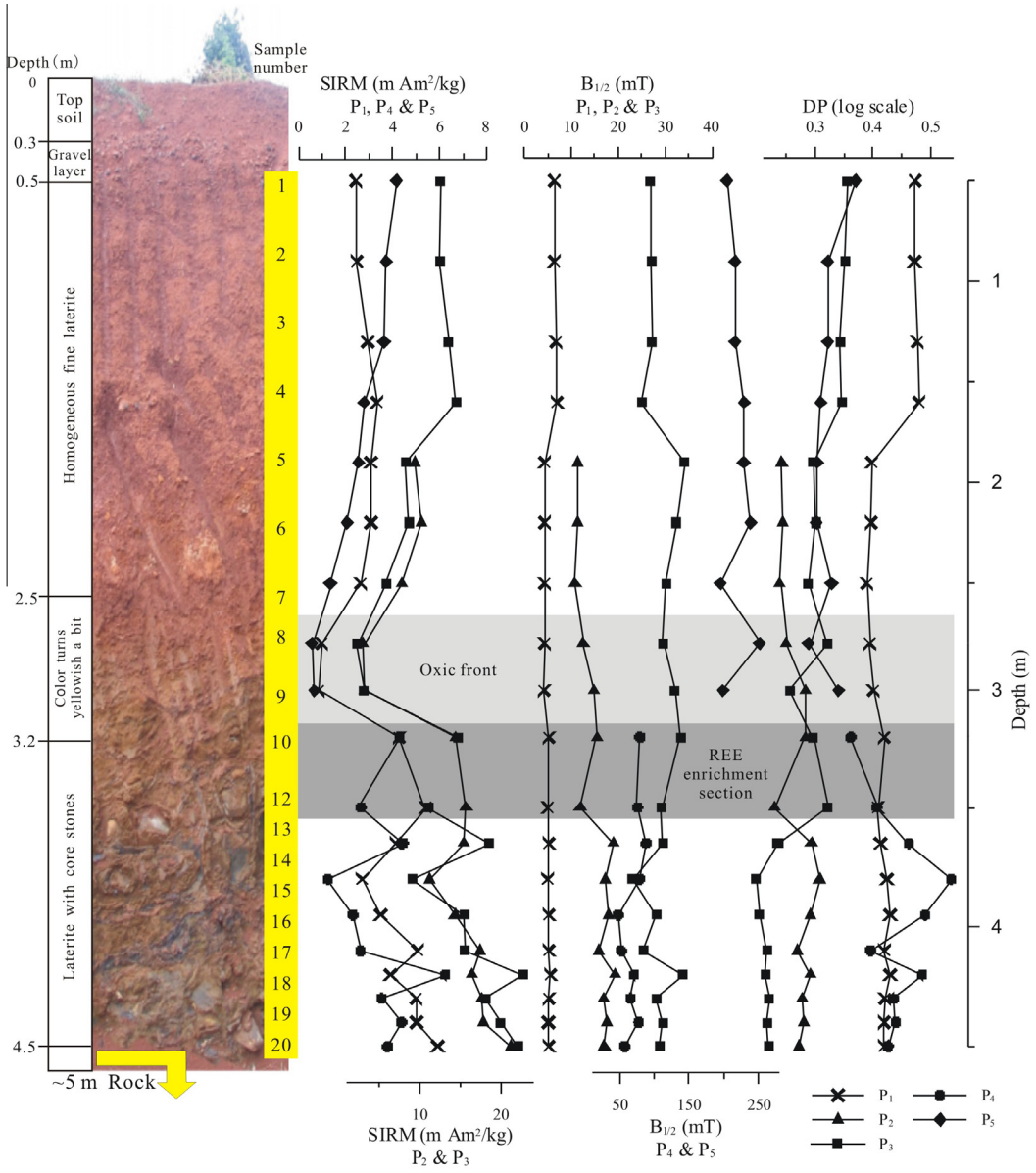

Fig. 6. Variations in fitted IRM parameters as a function of depth. The shaded bars represent the oxic front and REE enrichment sections defined by Ma et al. (2007). Explanation of each magnetic component as in Fig. 5.

The studied profile shows a continuous decrease in the S_{-300} from bottom to top (Fig. 7). This pattern supports the hysteresis and IRM data presented above and indicates the development of a hard magnetic component with increased weathering through the profile.

The concentration-dependent magnetic parameters χ, ARM and SIRM exhibit similar trends through the profile (Thompson and Oldfield, 1986; Oldfield, 1991; Verosub and Roberts, 1995; Evans and Heller, 2003; Liu et al., 2012c). The concentration of ferrimagnetic minerals appears to be highest around 3.5 m and drops rapidly to a minimum at ~3.0 m (Fig. 7). Above ~2.0 m, χ, ARM and SIRM achieve stable values, which decrease gradually in concert with the decreasing *S*-ratio. The position of the oxic front defined by Ma et al. (2007) is consistent with the minima in concentration-dependent magnetic parameters at ~3.0 m. At the assembly depth (3.2–3.5 m) (REE enrichment section defined by Ma et al. (2007)) most major and trace elements and enriched (Ma et al., 2007) and χ, χ_{fd}, ARM and SIRM all achieve high values indicating the neoformation of magnetic minerals as a product of pedogenesis (Fig. 7).

4.2. Magnetic grain size

Hysteresis parameters are indicative of mean domain state in magnetic mineral assemblages (Day et al., 1977; Dunlop, 2002). The ratios of Bcr/Bc and Mrs/Ms for the parent material are 1.56 and 0.50, respectively, indicating a predominantly stable single domain (SSD) assemblage (Fig. 8). Using the binary mixing lines of Dunlop (2002) as a general guide, the samples from the basalt profile contain varying amounts of superparamagnetic (SP) and stable SD particles. According to their position in the Day plot, samples 10 and 12 (3.2–3.5 m) appear to have the highest relative abundance of SP particles, which is supported by their elevated χ_{fd} values. However, most of the samples lie below the SP mixing line, suggesting that they may also contain a PSD component.

The magnetic grain-size proxies χ_{ARM}/χ and χ_{ARM}/SIRM show little variability (slight increase) between 0.5 and 3.5 m. The values transition between 3.5 m and 3.65 m and exhibit stable lower values at the bottom of the profile (Fig. 7). These patterns indicate that on average the magnetic mineral assemblage becomes finer

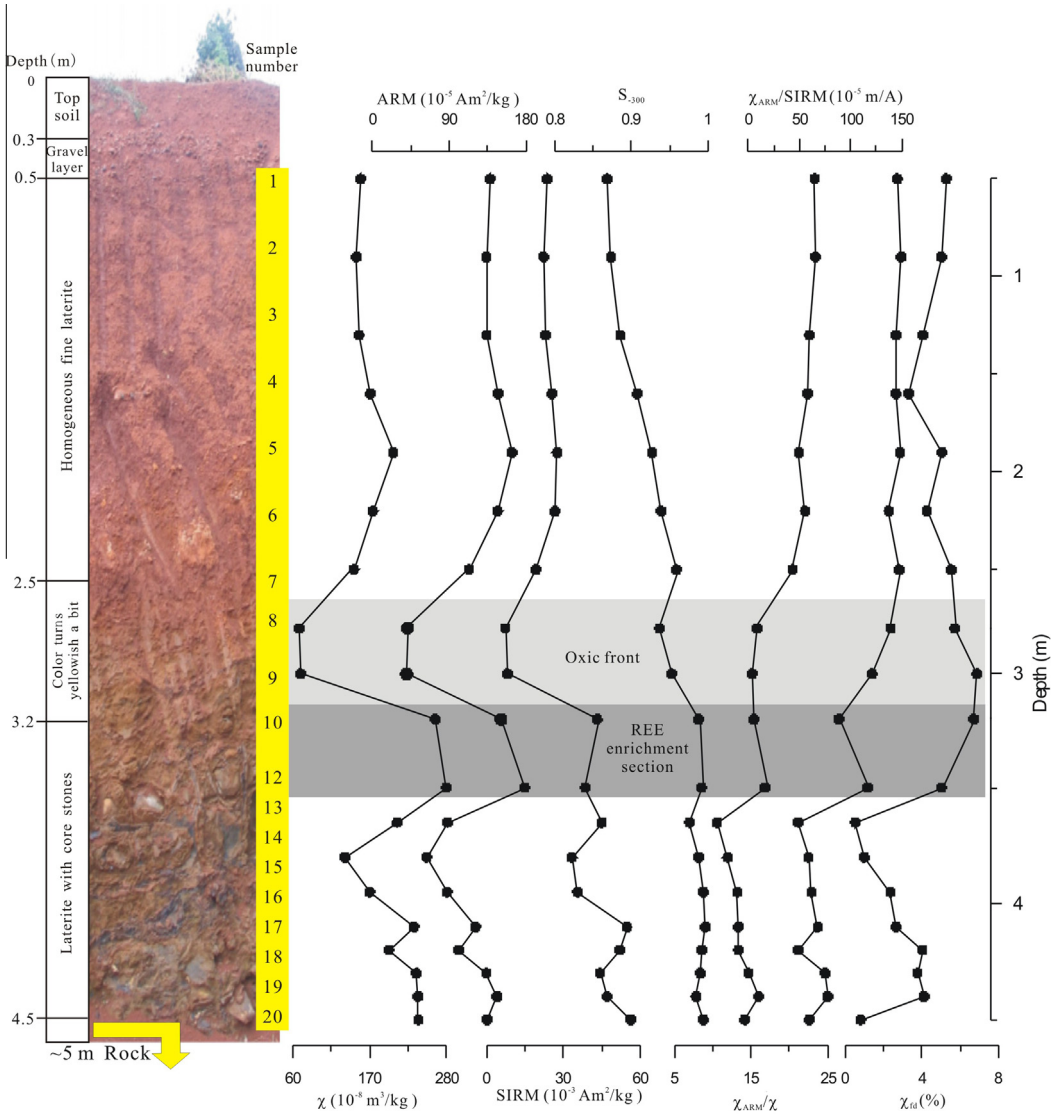

Fig. 7. Vertical variations of magnetic properties. The shaded bars represent the oxic front and REE enrichment sections defined by Ma et al. (2007).

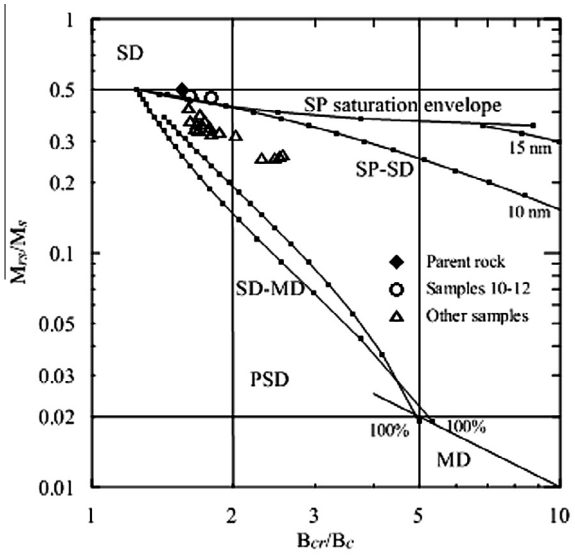

Fig. 8. Domain state determination using Day-plot (Dunlop, 2002).

through the section, which is consistent with the pedogenic formation of fine grained secondary ferrimagnets as a product of the weathering process. This pattern is supported by $\chi_{fd,}$ which is higher above 3.5 m, indicating a significant contribution from SP magnetic particles, a known product of pedogenesis (Thompson and Oldfield, 1986; Oldfield, 1991; Evans and Heller, 2003; Liu et al., 2012c) (Fig. 7). The variations identified in magnetic particle size on the basis on bulk magnetic parameters are consistent with those recognized in the FORC distributions described above (Fig. 4).

4.3. Magnetism–climate relationship

The bottom part of the profile (3.2–4.5 m) with unweathered core stones due to weak weathering can be called weathering crust with variety magnetic minerals, two different coercivity magnetite components, maghemite, and titanomaghemite (Figs. 5 and 6). As weathering process strengthened, strongly and extremely weathered parts were formed at middle part (1.9–3.0 m) and the upper part (0.5–1.6 m) of the weathering profile, respectively. The titanomaghemite magnetic phase is absent from the middle and upper parts of the profile due to highly weathering process under hot and humid tropical condition. On the other hand, a higher coer-

civity hematite magnetic phase is appeared at the middle and upper parts of the profile. Moreover, SIRM and DP patterns in Fig. 6 indicated that content and grain size of maghemite and hematite became higher and finer from the strongly weathered part to the extremely weathered part. These results indicated that weathering process under hot and humid tropical condition led to the neoformation of fine grained magnetic mineral phased and promoted mineral transformations in the form of maghemitization and hematization. The weathering degree of middle and upper parts of the studied profile may be corresponding to the weakly weathered and highly developed soil profiles at eastern Zhejiang province of China mentioned by Lu et al. (2008). Compared to their results, magnetic mineral composition of extreme weathering is consistent to the results from Lu et al. (2008). However, pedogenic hematite was also presented at the middle part of the present studied weathering profile (Fig. 6), indicating that relatively higher temperature and more rainfall at the study area promoted mineral transformation of hematization.

Vertical variations of magnetic properties illustrated in Fig. 7 also implied the influence of tropical climate on magnetic mineral development and weathering degree. As Ma et al. (2007) identified, the oxic front in the middle profile coincided with high water content and the required oxygen was transported by groundwater. Therefore, the REE enrichment section defined by Ma et al. (2007) (Figs. 6 and 7) should the boundary between strong weathering part and weathering crust and also the interface of groundwater seepage of the weathering profile since the parent basalt rock formation at ~4 Ma. Highest values of concentration dependent magnetic parameters c, ARM, and SIRM were appeared at the depths 3.2–3.5 m due to REE enrichment. Both content and grain size of magnetic particles maintain relatively stable for the upper part of the profile, indicating that almost the same weathering degree was led by hot and humid tropical condition for depths 0.5–1.6 m of the profile. For the middle part of the profile, magnetic mineral content decreased and particle size became coarser from 1.9 m to 3.0 m due to gradually weathering intensity.

5. Conclusions

The weathering of basaltic parent material in a humid tropical climate leads to the production of fine grained secondary ferrimagnets and increasing trends of maghemitization and hematization as weathering intensifies. Our results suggest that at certain stages of the weathering process titanomaghemite (produced by low temperature oxidation of the parent magnetic mineral assemblage) and pedogenic magnetite/maghemite coexist. In the upper section of the profile, where weathering is the most extreme, persistent low temperature oxidation leads to the dominance of maghemite and high coercivity hematite.

Proxies of magnetic grain-size indicate that the magnetic mineral assemblage fines with increasing weathering intensity. This is mainly attributed to the neoformation of fine grained magnetite particles as a product of the ongoing pedogenic process. Bulk magnetic parameters and FORC distributions from selected samples indicate that the magnetic grain-size varies from a combination of PSD and SD at the base of the profile, to SD at the middle, to a mixture of SP and SD in the upper zone.

In addition to gradual variations in magnetic particle relative abundance and size, concentration-dependent magnetic parameters (χ, ARM and SIRM) reveal specific zones where the magnetic mineral assemblage undergoes significant modification. Concentration-dependent parameters are highest at the assembly depth of major and trace elements and lowest at the oxic front when Fe content reaches a minimum. This demonstrates the complex response of magnetic mineral assemblages to weathering and the myriad of processes that exert an influence over both magnetic particle concentration and size.

Acknowledgments

Our work has benefitted from the support the support of the NSFC-Guangdong Joint Fund (Grant No. U1201131), the science and technology project of Guangdong province (Grant No. 2011B030500031) and the Guangdong Province, the Chinese Academy of Sciences comprehensive strategic cooperation project (Grant No. 2012B090400045). The authors also gratefully acknowledge the support of K.C. Wong Education Foundation, Hong Kong. Thanks are also due to Dr. David Heslop for his help in the preparation of this manuscript. We thank Chris Jones, Zhang K, and anonymous reviewers for their critical insights that have improve the work presented here.

References

Balsam, W.L., Ji, J.F., Chen, J., 2004. Climatic interpretation of the Luochuan and Lingtai loess sections, China, based on changing iron oxide mineralogy and magnetic susceptibility. Earth Planet. Sci. Lett. 223, 335–348.

Banerjee, S.K., 2006. Environmental magnetism of nanophase iron minerals: testing the biomineralization pathway. Phys. Earth. Planet. Inter. 154, 210–221.

Barrón, V., Torrent, J., 2002. Evidence for a simple pathway to maghemite in Earth and Mars soils. Geochim. Cosmochim. Acta 66, 2801–2806.

Begét, J.E., Stone, D.B., Hawkins, D.B., 1990. Paleoclimatic forcing of magnetic susceptibility variations in Alaskan loess during the late quaternary. Geology 18, 40–43.

Bina, M.M., Prevot, M., 1989. Thermomagnetic investigations of titanomagnetite in submarine basalts: evidence for differential maghemitization. Phys. Earth. Planet. Inter. 54, 169–179.

Bleil, U., Petersen, N., 1983. Variation in magnetization intensity and low temperature titanomagnetite oxidation of ocean floor basalts. Nature 301, 384–388.

Blundell, A., Dearing, J.A., Boyle, J.F., Hannam, J.A., 2009. Controlling factors for the spatial variability of soil magnetic susceptibility across England and Wales. Earth-Sci. Rev. 95, 158–188.

Borges, J.F.M., Hneda, M.L., Brinatti, A.M., da Cunha, J.B.M., Rosa, J.A., Fabris, J.D., 2011. Mössbauer analysis of high-energy mechanical-milled sand fraction of a magnetic soil developing on basalt. Hyperfine Interact. 203, 9–15.

Carvallo, C., Roberts, A.P., Leonhardt, R., Laj, C., Kissel, C., Perrin, M., Camps, P., 2006. Increasing the efficiency of paleointensity analyses by selection of samples using first-order reversal curve diagrams. J. Geophys. Res. 111, B12103. http://dx.doi.org/10.1029/2005JB004126.

Chevrier, V., Mathe, P.E., Rochette, P., Gunnlaugsson, H.P., 2006. Magnetic study of an Antarctic weathering profile on basalt: implications for recent weathering on Mars. Earth Planet. Sci. Lett. 244, 501–514.

Chlachula, J.M., Evans, E., Rutter, N.W., 1998. A magnetic investigation of a late quaternary loess/palaeosol record in Siberia. Geophys. J. Int. 132, 128–132.

Day, R., Fuller, M., Schmidt, V.A., 1977. Hysteresis properties of titanomagnetites: grain-size and compositional dependence. Phys. Earth. Planet. Inter. 13, 260–267.

De Oliveira, M.T., Formoso, M.L.L., Da Costa Jr., M.I., Meunier, A., 2002. The titanomagnetite to titanomaghemite conversion in a weathered basalt profile from Southern Parana basin, Brazil. Clays Clay Miner. 50, 478–493.

Dearing, J.A., Hay, K.L., Baban, M.J., Huddleston, A.S., Wellington, E.M.H., Loveland, P.J., 1996. Magnetic susceptibility of soil: an evaluation of conflicting theories using a national data set. Geophys. J. Int. 127, 728–737.

Deng, C.L., Zhu, R.X., Verosub, K.L., Singer, M.J., Vidic, N.J., 2004. Mineral magnetic properties of loess/paleosol couplets of the central loess plateau of China over the last 1.2 Myr. J. Geophys. Res. 109, B01103. http://dx.doi.org/10.1029/2003JB002532.

Deng, C.L., Vidic, N.J., Verosub, K.L., Singer, M.J., Liu, Q.S., Shaw, J., Zhu, R.X., 2005. Mineral magnetic variation of the Jiaodao Chinese loess/paleosol sequence and its bearing on long-term climatic variability. J. Geophys. Res. 110, B03103. http://dx.doi.org/10.1029/2004JB003451.

Dietze, F., Kontny, A., Heyde, I., Vahle, C., 2011. Magnetic anomalies and rock magnetism of basalts from Reykjanes (SW-Iceland). Stud. Geophys. Geod. 55, 109–130.

Dunlop, D.J., 2002. Theory and application of the Day plot (M_{rs}/M_s versus H_{cr}/H_c). 2. Application to data for rocks, sediments, and soils. J. Geophys. Res. 107, B3. http://dx.doi.org/10.1029/2001JB000487.

Egli, R., Chen, A.P., Winklhofer, M., Kodama, K.P., Horng, C.S., 2010. Detection of noninteracting single domain particles using first-order reversal curve diagrams. Geochem. Geophys. Geosyst. 11, 1. http://dx.doi.org/10.1029/2009GC002916.

Evans, M.E., Heller, F., 2003. Environmental Magnetism: Principles and Application of Environmagnetics. Academic Press, San Diego.

Fine, P., Singer, M.J., La Ven, R., Verosub, K.L., Southard, R.J., 1989. Role of pedogenesis in distribution of magnetic susceptibility in two California chronosequences. Geoderma 44, 287–306.
Gunnlaugsson, H.P., Helgason, O., Kristjansson, L., Nornberg, P., Rasmussen, H., Steinporsson, S., Weyer, G., 2006. Magnetic properties of olivine basalt: application to Mars. Phys. Earth. Planet. Inter. 154, 276–289.
Gunnlaugsson, H.P., Weyer, G., Helgason, O., 2002. Titanomaghemite in Icelandic basalt: possible clues for the strongly magnetic phase in Martian soil and dust. Planet. Space Sci. 50, 157–161.
Han, J.M., Lü, H.Y., Wu, N.Q., Guo, Z.T., 1996. The magnetic susceptibility of modern soils in China and its use for paleoclimate reconstruction. Stud. Geophys. Geod. 40, 262–275.
Hairrison, R.J., Feinberg, J.M., 2008. FORCinel: an improved algorithm for calculating first-order reversal curve distributions using locally weighted regression smoothing. Geochem. Geophys. Geosyst. 9, Q05016. http://dx.doi.org/10.1029/2008GC001987.
Heller, F., Shen, C.D., Beer, J., Liu, X.M., Liu, T.S., Bronger, A., Suter, M., Bonali, G., 1993. Quantitative estimates of pedogenic ferromagnetic mineral formation in Chinese loess and paleoclimatic implications. Earth Planet. Sci. Lett. 114, 385–390.
Heslop, D., Dekkers, M.J., Kruiver, P.P., Oorschot, I.H.M., 2002. Analysis of isothermal remanent magnetization acquisition curves using the expectation–maximization algorithm. Geophys. J. Int. 148, 58–64.
Heslop, D., McIntosh, G., Dekkers, M.J., 2004. Using time- and temperature-dependent Preisach models to investigate the limitations of modeling isothermal remanent magnetization acquisition curves with cumulative log Gaussian functions. Geophys. J. Int. 157, 55–63.
Ho, K.S., Chen, J.C., Juang, W.S., 2000. Geochronology and geochemistry of late Cenozoic basalts from the Leiqiong area, southern China. J. Asian Earth Sci. 18, 307–324.
Hu, X.F., Wei, J., Xu, L.F., Zhang, G.L., Zhang, W.G., 2009. Magnetic susceptibility of the quaternary Red Clay in subtropical China and its paleoenvironmental implications. Palaeogeogr. Palaeoclimatol. Palaeoecol. 279, 216–232.
Huang, Z.G., Cai, F.X., Han, Z.Y., Chen, J.H., Zong, Y.Q., Lin, X.D., 1993. Quaternary Volcano in Leizhou Peninsula and Hainan Island. Science Press, Beijing (in Chinese).
Jiang, Z.X., Liu, Q.S., Zhao, X.Y., Jin, C.S., Liu, C.C., Li, S.H., 2014. Thermal magnetic behavior of Al-substituted haematite mixed with clay minerals and its geological significance. Geophys. J. Int. 200, 130–143.
Koch, C.B., Morup, S., Madsen, M.B., Vistisen, L., 1995. Iron-containing weathering products of basalt in a cold, dry climate. Chem. Geol. 122, 109–119.
Kruiver, P.P., Dekkers, M.J., Heslop, D., 2001. Quantification of magnetic coercivity components by the analysis of acquisition curves of isothermal remanent magnetization. Earth Planet. Sci. Lett. 189, 269–276.
Kukla, G., Heller, F., Liu, X.M., 1988. Pleistocene climates in China dated by magnetic susceptibility. Geology 16, 811–814.
Lattard, D., Engelmann, R., Kontny, A., Sauerzapf, U., 2006. Curie temperatures of synthetic titanomagnetites in the Fe–Ti–O system: effects of composition, crystal chemistry, and thermomagnetic methods. J. Geophys. Res. 111, B12S28. http://dx.doi.org/10.1029/2006JB004591.
Liu, C.C., Deng, C.L., Liu, Q.S., Zheng, L.T., Wang, W., Xu, X.M., Huang, S., Yuan, B.Y., 2010. Mineral magnetism to probe into the nature of palaeomagnetic signals of subtropical red soil sequences in southern China. Geophys. J. Int. 181, 1395–1410.
Liu, C.C., Deng, C.L., Liu, Q.S., 2012b. Mineral magnetic studies of the vermiculated red soils in southeast China and their paleoclimatic significance. Palaeogeogr. Palaeoclimatol. Palaeoecol. 329–330, 173–183.
Liu, Q.S., Banerjee, S.K., Jackson, M.J., Deng, C.L., Pan, Y.X., Zhu, R.X., 2005a. Inter-profile correlation of the Chinese loess/paleosol sequences during Marine Oxygen Isotope Stage 5 and indications of pedogenesis. Quat. Sci. Rev. 24, 195–210.
Liu, Q.S., Deng, C.L., Yu, Y.J., Torrent, J., Jackson, M.J., Banerjee, S.K., Zhu, R.X., 2005b. Temperature dependence of magnetic susceptibility in an argon environment: implications for pedogenesis of Chinese loess/palaeosols. Geophys. J. Int. 161, 102–112.
Liu, Q.S., Roberts, A.P., Larrasoaña, J.C., Banerjee, S.K., Guyodo, Y., Tauxe, L., Oldfield, F., 2012c. Environmental magnetism: principles and applications. Rev. Geophys. 50, RG4002. http://dx.doi.org/10.1029/2012RG000393.
Liu, X.M., Liu, Z., Lü, B., Markovic, S.B., Chen, J.S., Guo, H., Ma, M.M., Zhan, G.Y., Feng, H., 2012a. The magnetic properties of Serbian loess and its environmental significance. Chin. Sci. Bull. 58, 353–363.
Liu, X.M., Rolph, T., Bloemendal, J., 1995. Quantitative estimates of paleoprecipitation at Xifeng, in the loess Plateau of China. Palaeogeogr. Palaeoclimatol. Palaeoecol. 113, 243–248.
Liu, X.M., Rolph, T., An, Z.S., Hesse, P., 2003. Paleoclimatic significance of magnetic properties on the Red Clay underlying the loess and paleosols in China. Palaeogeogr. Palaeoclimatol. Palaeoecol. 199, 153–166.
Long, X.Y., Ji, J.F., Balsam, W., 2011. Rainfall-dependent transformations of iron oxides in a tropical saprolite transect of Hainan Island, South China: spectral and magnetic measurements. J. Geophys. Res. 116, F03015. http://dx.doi.org/10.1029/2010JF001712.
Lu, S.G., Xue, Q.F., Zhu, L., Yu, J.Y., 2008. Mineral magnetic properties of a weathering sequence of soils derived from basalt in Eastern China. Catena 73, 23–33.
Ma, J.L., Wei, G.J., Xu, Y.G., Long, W.G., Sun, W.D., 2007. Mobilization and re-distribution of major and trace elements during extreme weathering of basalt in Hainan Island, South China. Geochim. Cosmochim. Acta 71, 3223–3237.
Maher, B.A., Thompson, R., 1992. Paleoclimatic significance of the mineral magnetic record of the Chinese loess and paleosols. Quat. Res. 37, 155–170.
Maher, B.A., Thompson, R., 1994. Pedogenesis and paleoclimate-interpretation of the magnetic susceptibility record of Chinese loess-paleosol sequences-comment. Geology 22, 857–858.
Maher, B.A., Thompson, R., 1995. Paleorainfall reconstructions from pedogenic magnetic susceptibility variations in the Chinese loess and paleosols. Quat. Res. 44, 383–391.
Maher, B.A., 1998. Magnetic properties of modern soils and quaternary loessic paleosols: paleoclimatic implications. Palaeogeogr. Palaeoclimatol. Palaeoecol. 137, 25–54.
Maher, B.A., 2007. Environmental magnetism and climate change. Contemporary Phys. 48, 247–274.
Maher, B.A., Alekseev, A., Alekseeva, T., 2003. Magnetic mineralogy of soils across the Russian steppe: climate dependence of pedogenic magnetite formation. Palaeogeogr. Palaeoclimatol. Palaeoecol. 201, 321–341.
Marshall, M., Cox, A., 1972. Magnetic changes in Pillow basalt due to sea floor weathering. J. Geophys. Res. 77, 6459–6469.
Morup, S., Saksager, O., Madsen, M.B., Bentzon, M.D., Koch, C.J.W., 1990. Weathering of basalt in an arctic climate. Hyperfine Inter. 57, 2269–2274.
Muxworthy, A.R., Dunlop, D.J., 2002. First-order reversal curve (FORC) diagrams for pseudo-single-domain magnetites at high temperature. Earth Planet. Sci. Lett. 203, 369–382.
Navarre-Sitchler, A., Brantley, S., 2007. Basalt weathering across scales. Earth Planet. Sci. Lett. 261, 321–334.
O'Donovan, J.B., O'Reilly, W., 1977. Range of non-stoichiometry and characteristic properties of the products of laboratory maghemitization. Earth Planet. Sci. Lett. 34, 291–299.
Oldfield, F., 1991. Environmental magnetism – a personal perspective. Quat. Sci. Rev. 10, 73–85.
Oliva-Urcia, B., Kontny, A., Vahle, C., Schleicher, A.M., 2011. Modification of the magnetic mineralogy in basalts due to fluid–rock interactions in a high-temperature geothermal system. Geophys. J. Int. 186, 155–174.
Özdemir, Ö., 1987. Inversion of titanomaghemites. Phys. Earth. Planet. Inter. 46, 184–196.
Petrovsky, E., Kapicka, A., 2006. On determination of the curie point from thermomagnetic curves. J. Geophys. Res. 111, B12S27. http://dx.doi.org/10.1029/2006JB004507.
Pike, C.R., Roberts, A.P., Dekkers, M.J., Verosub, K.L., 2001. An investigation of multi-domain hysteresis mechanisms using FORC diagrams. Phys. Earth. Planet. Inter. 126, 11–25.
Pike, C.R., Roberts, A.P., Verosub, K.L., 1999. Characterizing interactions in fine magnetic particle systems using first order reversal curves. J. Appl. Phys. 85, 6660–6667.
Porter, S.C., Hallet, B., Wu, X., An, Z., 2001. Dependence of near-surface magnetic susceptibility on dust accumulation rate and precipitation on the Chinese Loess Plateau. Quat. Res. 55, 271–283.
Roberts, A.P., Pike, C.R., Verosub, K.L., 2000. First-order reversal curve diagrams: a new tool for characterizing the magnetic properties of natural samples. J. Geophys. Res. 105 (B102), 28461–28475.
Schwertmann, U., 1985. The effect of pedogenic environments on iron oxide minerals. Adv. Soil Sci. 1, 171–200.
Singer, M.J., Verosub, K.L., Fine, P., TenPas, J., 1996. A conceptual model for the enhancement of magnetic susceptibility in soils. Quat. Int. 34, 243–248.
Soubrand-Colin, M., Horen, H., Courtin-Nomade, A., 2009. Mineralogical and magnetic characterization of iron titanium oxides in soils developed on two various basaltic rocks under temperate climate. Geoderma 149, 27–32.
Spassov, S., Heller, F., Kretzschmar, R., Evans, M.E., Yue, L.P., Nourgaliev, D.K., 2003. Detrital and pedogenic magnetic mineral phases in the loess/palaeosol sequence at Lingtai (Central Chinese Loess Plateau). Phys. Earth. Planet. Inter. 140, 255–275.
Stober, J.C., Thompson, R., 1977. Palaeomagnetic secular variation studies of Finnish lake sediment and the carriers of remanence. Earth Planet. Science Lett. 37, 139–149.
Thompson, R., Oldfield, F., 1986. Environmental Magnetism. Allen & Imwin, London.
Van Dam, R.L., Bruce, J., Harrison, J., Hirschfeld, D.A., Meglich, T.M., Li, Y.G., North, R.E., 2008. Mineralogy and magnetic properties of basaltic substrate soils: Kaho'olawe and Big Island, Hawaii. Soil Sci. Soc. Am. J. 72, 244–257.
Verosub, K.L., Roberts, A.P., 1995. Environmental magnetism: past, present, and future. J. Geophys. Res. 100, 2175–2192.
Warrier, A.K., Shankar, R., 2009. Geochemical evidence for the use of magnetic susceptibility as a paleorainfall proxy in the tropics. Chem. Geol. 265, 553–562.
Yin, Q.Z., Guo, Z.T., 2006. Mid-Pleistocene vermiculated red soils in southern China as an indication of unusually strengthened East Asian monsoon. Chin. Sci. Bull. 51, 213–220.
Zhang, C.X., Paterson, G.A., Liu, Q.S., 2012. A new mechanism for the magnetic enhancement of hematite during heating: the role of clay minerals. Stud. Geophys. Geod. 56, 845–860.
Zhou, L.P., Oldfield, F., Wintle, A.G., Robinson, S.G., Wang, J.T., 1990. Partly pedogenic origin of magnetic variations in Chinese loess. Nature 346, 737–739.
Zhou, W., Van der Voo, R., Peacor, D.R., 1997. Single-domain and superparamagnetic titanomagnetite with variable Ti-content in young ocean-floor basalts: no evidence for rapid alteration. Earth Planet. Science Lett. 150, 353–362.
Zhu, B.Q., Wang, H.F., 1989. Nd–Sr–Pb isotopic and chemical evidence for the volcanism with MORB-OIB source characteristics in the Leiqiong Area, China. Geochimica 18, 193–201.